JOURNAL OF MATERIALS SCIENCE 31 (1996) 1595–1602

Phase transformations of δAl_2O_3 (Saffil) fibres during their interaction with molten MgLi alloys

S. KÚDELA, V. GERGELY
Institute of Materials and Machine Mechanics, Slovak Academy of Sciences, 83606 Bratislava, Slovakia

L. SMRČOK
Institute of Inorganic Chemistry, Slovak Academy of Sciences, 84236 Bratislava, Slovakia

S. OSWALD, S. BAUNACK, K. WETZIG
Institute for Solid State Analytics and Structural Research at the Institute for Solid State and Materials Research, Post box 270016, D-01171 Dresden, Germany

The phase transformation of δAl_2O_3 occurring in Saffil fibres during their infiltration with molten Mg–8 wt% Li alloy was studied by secondary ion mass spectroscopy, X-ray diffraction and infrared spectroscopy methods. It has been shown, that lithium penetrates very quickly into the whole fibre volume, attaining up to Li/Al $\approx$ 0.25–0.30 ion ratio. The metastable spinel-like compound, γ(Li), was formed by incorporation of Li^+ ions into the δAl_2O_3 lattice in which the basic spinel structure unit has been assigned by the formula $Al_8\,[Al_{(40-x)/3}\square_{(8-2x)/3}Li_x]O_{32}$. During long-term annealing, a further transformation $\gamma(Li) \rightarrow LiAl_5O_8$ proceeded, and $LiAlO_2$ aluminate was also identified in Saffil fibres with high Li/Al concentration ratio values. In parallel with lithium, magnesium also penetrated the Saffil fibres within an infiltration period; however, the incorporation of magnesium into the spinel lattice has not been observed.

1. Introduction

The Saffil* fibres (SF), which have been developed specially for an application in metal matrix composites, are widely used as the reinforcements in light metal matrices (aluminium, magnesium and their alloys) [1]. A dominant structural component of SF are the δAl_2O_3 crystallites which represent a metastable transitive alumina product of the böhmite γAlOOH irreversible transformation towards αAl_2O_3 occurring at temperatures of 873–1173 K

$$\gamma AlOOH \rightarrow \gamma Al_2O_3 \rightarrow \delta Al_2O_3 \rightarrow \Theta Al_2O_3 \rightarrow \alpha Al_2O_3 \quad (1)$$

As far as the ΘAl_2O_3 stage, this transformation sequence proceeds within a framework of an approximately cubic close-packed oxygen sublattice and it may be ideally accomplished solely by an Al^{3+} cation migration and ordering process [2]. The δ-Al_2O_3 phase is a superstructure of three tetragonally distorted spinel cells with cell parameters $c_\delta \approx 3c_\gamma$, $a_\delta \approx a_\gamma$ [3].

The pressure infiltration of SF preforms with MgLi alloys is a promising means of preparing the metal matrix composites combining very low density and satisfactory strength and deformation characteristics. The SF, however, are damaged in contact with molten MgLi alloys due to lithium penetration into the SF interior, resulting in their brittleness [4].

In a previous work [5] we have studied this interaction by different experimental methods, concluding that a gradual transformation of δAl_2O_3 lattice towards the spinel $LiAl_5O_8$ took place where some of the Li^+ ions were assumed to be substituted by Mg^{2+}. In the same paper, the model of this interaction was discussed, assuming that lithium penetrates along δAl_2O_3 grain boundaries forming Li_2O, and consequently Li^+ diffuses into the tetragonal δAl_2O_3 lattice gradually occupying the vacant octahedral sites by ion exchange $Al^{3+} + 2\square = 3Li^+$ forming the mixed Al_2O_3–$LiAl_5O_8$ spinel compound, γ(Li), which can be transformed to the lithium spinel $LiAl_5O_8$ in the final stage.

To make this model conception more precise, or if need be to correct it, we have investigated in more detail the $\delta Al_2O_3 \rightarrow LiAl_5O_8$ transformation by means of secondary ion mass spectrometry (SIMS), X-ray diffraction (XRD) and infrared spectroscopy (IR) methods using the SF, that were extracted from SF/Mg8Li-type composite samples by dissolution of MgLi matrix, which represent different interaction stages.

*Saffil is the Trademark of Imperial Chemistry Industries plc for their alumina fibres.

0022–2461

2. Experimental procedure

2.1. Saffil/Mg8Li composites fabrication

The samples of SF/Mg8Li type composite materials were prepared in the same way as described in more detail elsewhere [5], i.e. by pressure infiltration of SF preform in an autoclave under an argon pressure (up to 6 MPa) at temperatures of 888–908 K and contact times of 4–30 s, and also extremely at 918 K/420 s. The contact time is defined as the interval between the start of argon pressure application and a sample pulling out from the molten metal bath. The SF preform (Saffil RF grade, ICI, Runcorn, UK) contained about 20 vol % alumina fibres and about 3–4 wt % SiO_2 binder. The alumina fibres have a polycrystalline structure (~ 50 nm crystallites size) in which δAl_2O_3 as the predominant phase contains a small amount of silica (3–4 wt %) to stabilize the δ polymorphism and inhibit crystallite coarsening [6]. The Mg–8 wt % Li matrix alloy was prepared by alloying of magnesium (purity 99.9%) with lithium (purity 99.95%) under an argon pressure.

2.2. Fibre extraction

The as-prepared composite material samples were dissolved in 10 %Br–CH_3COOCH_3 solution at its boiling point and extracted SF were then centrifugally separated and decanted.

2.3. Secondary ion mass spectrometry

The as-extracted SF were mechanically impressed into indium foil (purity 99.99%) and analysed by the SIMS method (IMMA, Applied Research Laboratories, USA). For the measurement of elemental depth profiles or intensity versus time profiles, respectively, the emitted secondary ions were taken from an area of $30 \times 30\ \mu m^2$ covered by the extracted fibres during sputtering an area of $60 \times 60\ \mu m^2$ with Ar^+ ions for about 60 min at 18.5 keV and 40 nA.

2.4. Infrared spectroscopy

The infrared spectra were recorded from extracted SF on JFS 66v set with a Fourier transform–infrared spectrometer (Bruker) in the wave number range 400–900 cm^{-1}. The studied fibres were dispersed in paraffin oil (Nujol).

2.5. X-ray diffraction

Transmission X-ray diffraction patterns of the SF samples were taken using the Stoe Stadi P system with CoK_α radiation.

3. Results

3.1. Secondary ion mass spectrometry (SIMS)

A typical morphology of SF extracted from Mg8Li matrix is shown in Fig. 1. The SIMS method was used

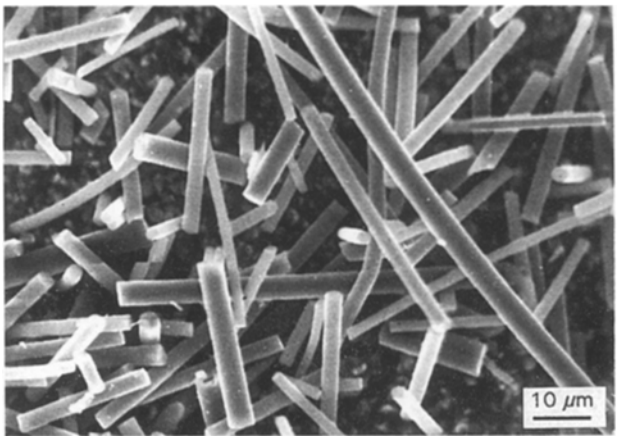

Figure 1 Scanning electron micrograph of SF extracted from Mg8Li matrix.

for semiquantitative determination of relative Li/Al and Mg/Al elemental concentrations in as-extracted SF by registration of $^7Li^+$, $^{24}Mg^+$, $^{25}Mg^+$ and $^{27}Al^+$ secondary ions and normalizing the calculation with an empirical sensitivity factor.

Fig. 2a and b show typical measured intensity versus time and calculated relative concentration profiles of the samples under investigation. In contrast with the strongly decreasing intensity profiles (more than one order of magnitude), the relative concentrations vary only in the surface region. It was impossible to perform a depth calibration of the intensity versus time profiles because of the irregular sputtering erosion of impressed SF.

In Fig. 3, eroded SF are shown in a sputtering crater area manifesting that the secondary ion mass spectra have been taken not only from the surface regions but gradually from the whole fibre volume. It corresponds to the results of sputtering experiments obtained by us from flat alumina samples exhibiting an erosion depth of about 1–2 μm under the same sputtering conditions. The intensity drop, which is evident in Fig. 2a, can be attributed to the removal of weakly embedded SF during the indium foil erosion.

In Table I the relative lithium and magnesium concentrations are presented that have been obtained from: (a) SF which were infiltrated with Mg8Li alloy at 888 and 908 K for 4, 15 and 30 s, as well as 918 K/420 s (b) from magnesium matrix-extracted SF (953 K/420 s) and, (c) virgin SF. The data in parentheses are the infiltration process variables (temperature/time). In both SF extracted from a magnesium matrix and virgin SF, lithium was detected in traces only. Nevertheless, already within the shortest contact time (4 s) a relatively large amount of lithium was accumulated in SF during their infiltration with Mg8Li alloy, suggesting a very fast lithium penetration into the SF interior.

As seen in Table I, in parallel with lithium, magnesium also penetrated in a significant amount into SF during their contact with molten Mg8Li alloy (up to $Mg/Al \approx 0.06$ concentration ratio – note that in the present paper all relative concentrations are given as ratios of atomic concentrations corresponding to the ion ratios from the chemical point of view) in dependence on the infiltration process variables (temperature,

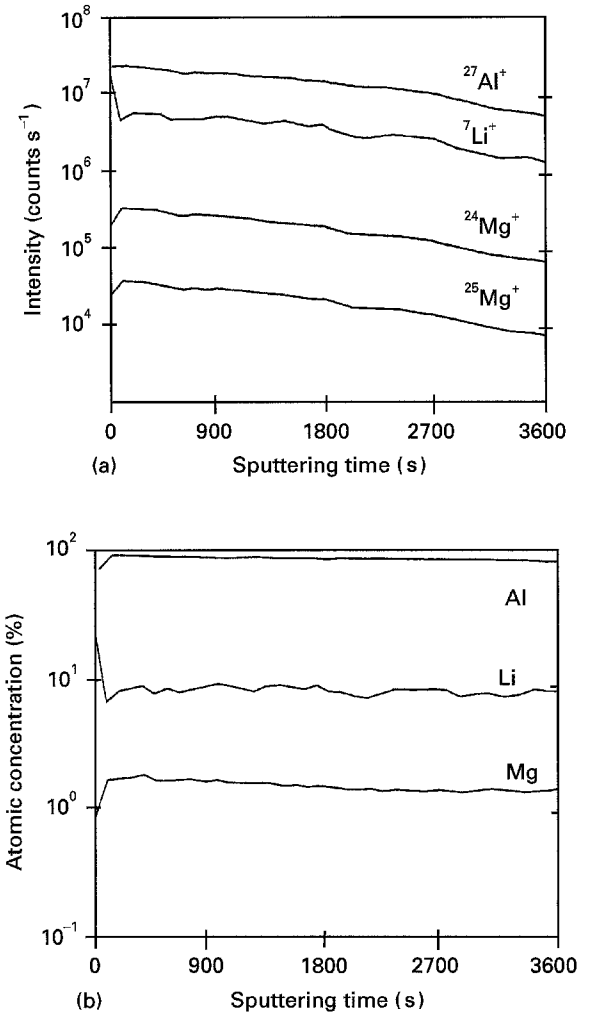

Figure 2 (a) Typical measured intensity versus time profiles of $^7Li^+$, $^{24}Mg^+$, $^{25}Mg^+$ and $^{27}Al^+$ secondary ions taken from as-extracted SF; (b) corresponding relative concentration versus time profiles.

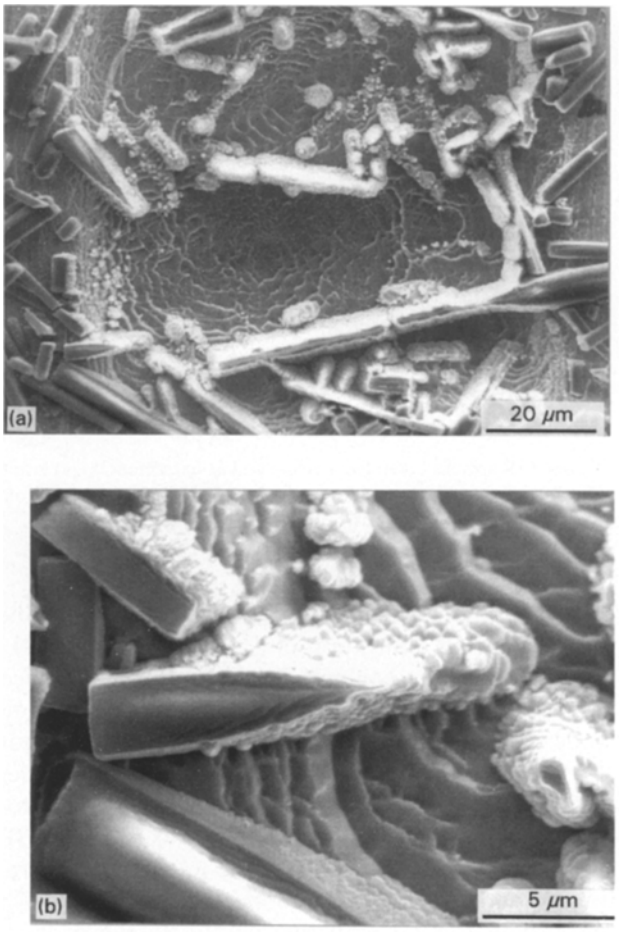

Figure 3 Scanning electron micrographs of eroded SF in a sputtering crater area: (a) micrograph from the whole crater region; (b) detail from the crater rim.

time). On the other hand, the magnesium concentration level in SF that were extracted from a magnesium matrix remained nearly the same as that in virgin SF, i.e. below the Mg/Al≈0.01 concentration ratio.

3.2. Infrared spectroscopy (IR)

In Fig. 4 the IR spectra, which were taken from virgin SF as well as those as-extracted from both magnesium (953 K/420 s) and Mg8Li matrices (888 K/4 s, and 918 K/420 s), are presented in the wave number range 400–900 cm^{-1}. There are at least five absorption bands resolvable in the IR spectrum belonging to the virgin SF (line a) : 560, 645, 721, 756 and 822 cm^{-1}. Some of them (560, 756 and 822 cm^{-1}) lie close to the principal bands reported for γAl_2O_3 [7] and θAl_2O_3 [8]. The band at 721 cm^{-1} is related to the Nujol spectrum [9], though we have also found the same band in SF treated by the KBr technique, i.e. this band is also inherent in the SF samples.

Considering that the δAl_2O_3 lattice contains both tetrahedral AlO_4 and octahedral AlO_6 coordination groups of the condensed type, consistent with the appearance of their spectral bands in the 500–680 cm^{-1} and 700–900 cm^{-1} regions [8], the 560 and 645 cm^{-1} bands should be related to the AlO_6 groups, whereas those at 721, 756 and 822 cm^{-1} should be related to the AlO_4 tetrahedra.

TABLE I Relative lithium and magnesium concentrations in as-extracted SF determined by the SIMS method

Infiltration process variables		Matrix	Ion ratio	
(K)	(s)		Li/Al	Mg/Al
953	420	Mg	< 0.001	0.007
888	4	Mg8Li	0.08	0.007
888	15		0.09	0.009
888	30		0.30	0.03
908	4	Mg8Li	0.10	0.02
908	15		0.09	0.03
908	30		0.25	0.06
918	420	Mg8Li	0.28	–
Virgin SF			< 0.001	0.007

Although throughout this series (lines a–d) both virgin and as-extracted SF manifest quite a similar feature of IR spectra, maintaining the chief absorption bands, a tendency to be less complex and more broad with the increase in lithium content is significant. In particular, the band at 560 cm^{-1} (lying between 400 and 700 cm^{-1}) becomes more intensive, extending towards lower frequencies (line d).

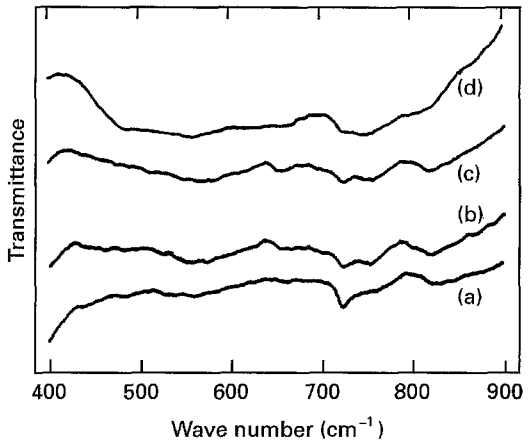

Figure 4 IR spectra taken from virgin and as-extracted SF: (a) virgin SF; (b) SF from a magnesium matrix (953 K/420 s); (c) SF from Mg8Li matrix (888 K/4 s); (d) SF Mg8Li matrix (918 K/420 s).

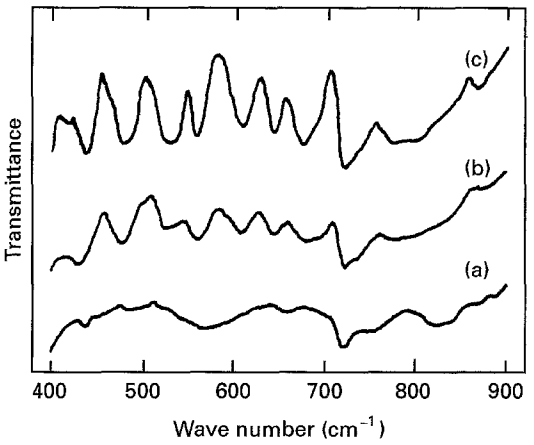

Figure 5 IR spectra taken from annealed both virgin and extracted SF: (a) virgin SF; (b) SF from Mg8Li matrix (888 K/4 s); (c) SF from Mg8Li matrix (918 K/420 s).

The lithium spinel $LiAl_5O_8$ was expected to be formed during infiltration of SF with molten Mg8Li alloy. However, a comparison of IR spectra obtained from as-extracted SF with those reported for both ordered and disordered $LiAl_5O_8$ spinel compounds [7, 10, 11] did not confirm this assumption. In order to identify the presence of lithium in SF by IR spectroscopy, the virgin and also some of the as-extracted SF were annealed at 1523 K/10 min in argon (spectral purity) and then cooled to room temperature for 10 h (according to [7]) with the aim to fix the ordered $LiAl_5O_8$ polymorphism displaying a characteristic extremely complex IR spectrum. The corresponding IR spectra are presented in Fig. 5 and the ordered $LiAl_5O_8$ compound occurrence is evident here, wherein the intensities of absorption bands seem to be correlated with lithium content (see Table I). Tarte [8] has attributed, by ^6Li–^7Li isotopic shift, the wave numbers of 490, 536, 561 and 614 cm^{-1} in ordered $LiAl_5O_8$ compound to the mixed (Al–O) + (Li–O) vibrations, and 647, 681, 729, 727 and 869 cm^{-1} to the pure Al–O stretch vibrations.

Fig. 6 shows the IR spectra belonging to the SF (infiltrated at 918 K/420 s) in both (a) as-extracted, and (b) annealed states. Absorption bands that were assigned by Tarte [8] for mixed (Al–O) + (Li–O) vibrations are marked by "×" in line (b). As seen, these mixed vibration modes are well fitted into the region of a broad absorption band, 400–700 cm^{-1} in line (a), which suggests that the above-mentioned changes in this absorption band (increased intensity, shift towards lower frequencies) can be attributed to the presence of randomly distributed Li^+ ions.

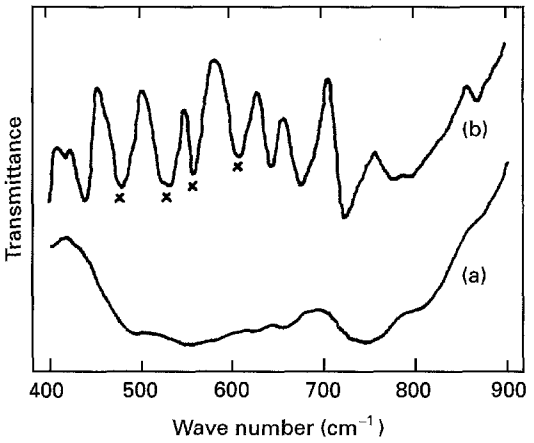

Figure 6 IR spectra taken from (a) as-extracted SF (918 K/420 s) and (b) annealed SF (918 K/420 s). Bands assigned by "x" correspond to the mixed (Al–O) + (Li–O) vibrations.

3.3. X-ray diffraction (XRD)

Complementary to the IR spectroscopy, the XRD measurements were performed with the same SF samples. In Fig. 7 the XRD patterns are presented which have been obtained from (a) virgin SF, (b) SF extracted from a magnesium matrix (953 K/420 s), (c–e) SF extracted from an Mg8Li matrix (888 K/4 s, 908 K/30 s, and 918 K/420 s), as a representative series of studied SF samples. In all XRD patterns, the strong 4 0 0 and 4 4 0 reflections are visible, originating chiefly from the oxygen fcc layers, which remain relatively unmoved from their positions in δAl_2O_3 superlattice suggesting the maintenance of elemental spinel cells during the infiltration process.

The 4 0 0/0 . 0 . 12 and 4 4 0/4 . 0.12 line splits indicate some tetragonal distortion of spinel cells belonging to the δAl_2O_3 superlattice in virgin SF. The gradual 0 . 0 . 1 2 → 4 0 0 and 4 . 0 . 1 2 → 4 4 0 lines confluences reflect the disappearance of planes with high indices as a result of δAl_2O_3 spinel cells tetragonal distortion removal. We have used the 0 . 0 . 1 2 → 4 0 0 lines confluence to demonstrate the dynamics of these processes. As seen in Fig. 8 there is no difference between SF infiltrated with pure magnesium (sample 2) and virgin SF (sample 1). Already a very short contact of SF with molten Mg8Li alloy (888 K/4 s) was distinctly displayed by the reduction in differences between 4 0 0 and 0 . 0 . 1 2 reflections (sample 3). On the other hand, within a relatively large interval of infiltration process variables (888 K/4 s–908 K/30 s), only the small changes in 0 . 0 . 1 2 → 4 0 0 confluence were observed (samples 3 and 4). The 0 . 0 . 1 2 line disappeared totally in the long-term infiltrated SF (sample 5).

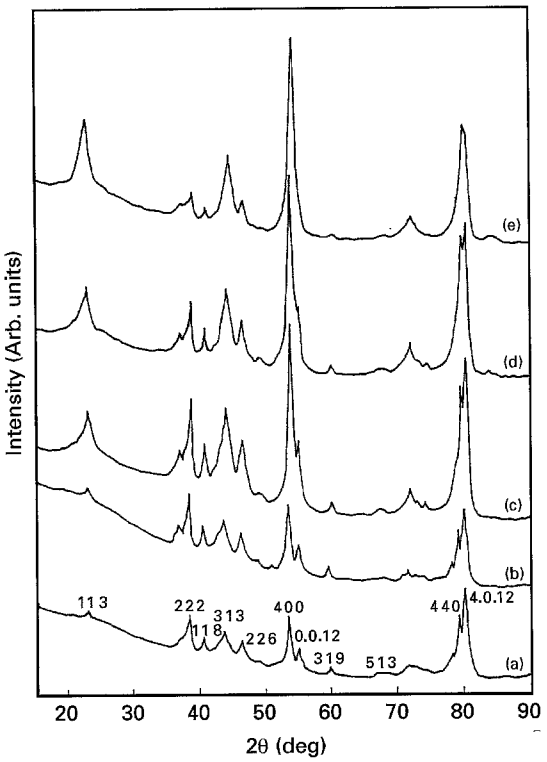

Figure 7 XRD patterns taken from virgin and as-extracted SF: (a) virgin SF; (b) SF from a magnesium matrix (953 K/420 s); (c) SF from Mg8Li matrix (888 K/4 s); (d) SF from Mg8Li matrix (908 K/30 s); (e) SF from Mg8Li matrix (918 K/420 s).

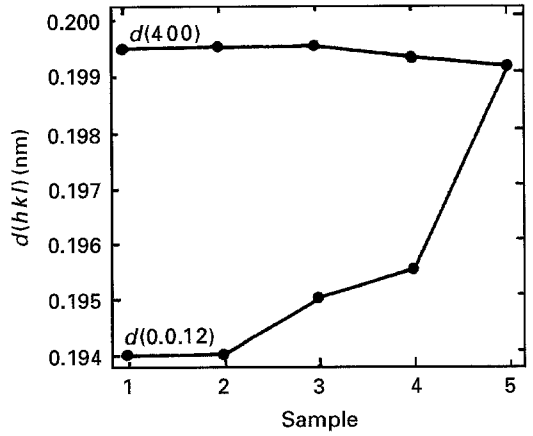

Figure 8 The $d_{4\,0\,0}$ and $d_{0.0.1\,2}$ values corresponding to XRD patterns in Fig. 7: (1) virgin SF; (2) SF from a magnesium matrix (953 K/420 s); (3) SF from Mg8Li matrix (888 K/4 s); (4) SF from Mg8Li matrix (908 K/30 s); (5) SF from Mg8Li matrix (918 K/420 s).

The diagram in Fig. 8 can be easily transformed to be in terms of a and $c/3$ cell parameter values which more explicitly show the tendency towards removal of tetragonal spinel cells distortion with increasing lithium content (Fig. 9). The changes towards an ideal cubic cell ($c/3a \rightarrow 1$) were accomplished mainly by increasing in the c parameter, while the a value remained quite unchanged, resulting in some volume expansion (about 2%) of spinel cells, as demonstrated by the dashed line diagram in Fig. 9. It should be noted that c and a have been calculated from 4 0 0 and 0.0.1 2 lines only.

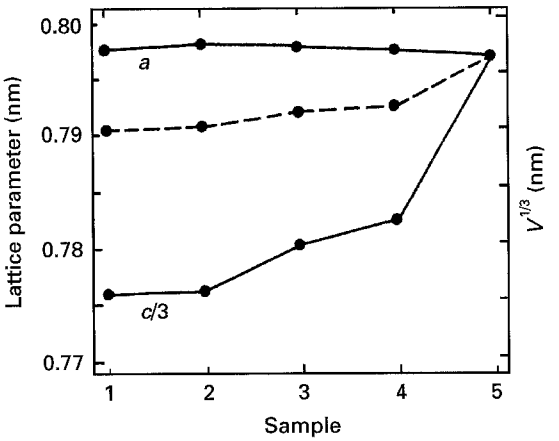

Figure 9 The a and $c/3$ cell parameters of the δAl_2O_3 superlattice, which correspond to the basic spinel structure unit, as well as (- - - -) its volume changes calculated from XRD patterns in Fig. 7. (1) virgin SF, (2) SF from a magnesium matrix (953 K/420 s), (3) SF from Mg8Li matrix (888 K/4 s), (4) SF from Mg8Li matrix (908 K/30 s), (5) SF from Mg8Li matrix (918 K/420 s).

Both 1 1 8 and 2 2 2 reflections are inherent in the δAl_2O_3 superlattice [12] and they cannot be simply reindexed in the f c c spinel cell. As seen in Fig. 7, the 1 1 8 and 2 2 2 lines are observed in a whole series of XRD patterns; nevertheless, $I_{1\,1\,8}$ and $I_{2\,2\,2}$ intensities are gradually weakened relative to the strongest $I_{4\,0\,0}$ line. On the other hand, the 2 2 0 reflection, which is typical for the f c c spinel cells, does not appear in the XRD patterns presented here; however, in some other samples of long-term infiltrated SF (918 K/420 s), the 2 2 0 line was identified. These facts indicate that during infiltration of SF with molten Mg8Li alloy, the decomposition of δAl_2O_3 superlattice into individual spinel cells occurs to a certain degree.

The XRD patterns taken from annealed SF (corresponding to IR spectra in Fig. 5) are presented in Fig. 10. The ordered $LiAl_5O_8$ spinel (cell parameter $a = 0.7905$ nm) was found in both short- (sample b) and long-term (sample c) infiltrated SF. In parallel with the $LiAl_5O_8$ compound, αAl_2O_3 was also identified in sample (b), whereas in sample (c) XRD lines belonging most probably to the $LiAlO_2$ aluminate were found. In the annealed virgin SF, the δ, θ and α-Al_2O_3 phases were detected, i.e. the incomplete transformation towards the stable α-Al_2O_3 phase proceeded here (sample a).

4. Discussion

The model of interaction of SF with molten MgLi alloys presented elsewhere [5] and briefly described in the opening part of this paper, is based on the assumption that lithium penetrates along δAl_2O_3 crystallite grain boundaries where the Li_2O oxide is formed by reduction of SiO_2 and Al_2O_3 and, consequently, Li^+ ions diffuse into δ-spinel cells to form the mixed oxide Al_2O_3-Li_2O. An ability of small alkali ions to penetrate the defective alumina spinel lattice is well known [13], and the available cation vacancies seem to play an important role there. As reported by Levy

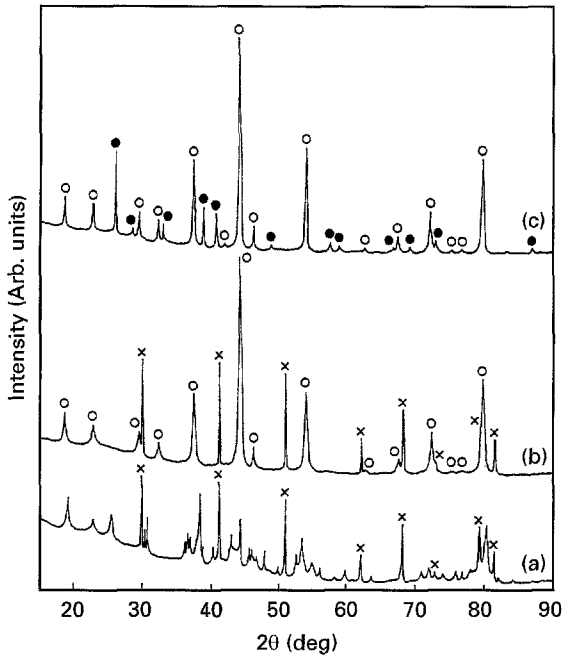

Figure 10 XRD patterns taken from annealed SF: (a) virgin SF, (b) SF extracted from Mg8Li matrix (888 K/4 s), (c) SF extracted from Mg8Li matrix (918 K/420 s). (×) αAl_2O_3, (○) $LiAl_5O_8$, (●) $LiAlO_2$. Unmarked lines in (a) belong to δ and θAl_2O_3.

and Bauer [14], Li^+ ions effectively fill the vacant sites in the γAl_2O_3 lattice, and in the case when the Li^+ concentration exceeds a ratio $Li/Al \approx 0.02$, occupation by lithium of sites other than the existing lattice vacancies, apparently begins to occur.

Both γ- and δAl_2O_3 are defective spinel compounds which differ from each other only in a cation arrangement. Table II shows the available and occupied cation sites for units of structure equivalent in size to the ideal spinel unit cell, presented by Wilson [2] for γ- and δ-aluminas.

If one accepts the octahedral ordering of cation vacancies in δAl_2O_3 and considers the result presented by Verwey and Heilmann [15], Li^+ ions can be incorporated into the δ-spinel lattice in two ways

$$x\mathrm{Li}^+ + \mathrm{Al}_8[\mathrm{Al}_{40/3}\square_{8/3}]\mathrm{O}_{32} \rightarrow \mathrm{Al}_8[\mathrm{Al}_{(40-x)/3}\square_{(8-2x)/3}\mathrm{Li}_x]\mathrm{O}_{32} + (x/3)\mathrm{Al}^{3+} \quad (2a)$$

$$x\mathrm{Li}^+ + \mathrm{Al}_8[\mathrm{Al}_{40/3}\square_{8/3}]\mathrm{O}_{32} \rightarrow \mathrm{Al}_{(24-x)/3}\mathrm{Li}_{x/3}[\mathrm{Al}_{40/3}\square_{8-2x)/3}\mathrm{Li}_{2x/3}]\mathrm{O}_{32} + (x/3)\mathrm{Al}^{3+} \quad (2b)$$

where the vacancy is denoted by the open square, and the terms in brackets represent octahedral cations or vacancies. In the reaction scheme 2a, Li^+ ions preferentially occupy the octahedral cation sites, whereas in scheme 2b, Li^+ ions are randomly distributed within spinel cells. Both the schemes lead to the mixed δAl_2O_3–$LiAl_5O_8$ spinel compounds, γ(Li), giving the different $LiAl_5O_8$ polymorphism of the order–disorder type in the final stage ($x = 4$). As the disordered $LiAl_5O_8$ is unstable below 1563 K [16], the alternative (2a) seems more probable to occur at infiltration temperatures (≤ 918 K).

The presence of cation vacancies in defective aluminas is displayed by tetragonal distortion of basic spinel cells ($c/a < 1$ for γAl_2O_3, and $c/3a < 1$ for δAl_2O_3). Wilson and McConnell [12] have shown that a pronounced tetragonally distorted spinel structure is formed in cases when the vacancies are predominantly concentrated on either tetrahedral (γAl_2O_3) or octahedral (δAl_2O_3) cation sites (Table II). A random distribution of vacancies tends to adjust the c/a ratio close to its "cubic" value with minimal tetragonal distortion degree. The ideal cubic state, however, is never reached because of the concurrent phenomenon of reordering on the octahedral sites [17]. In the reaction schemes 2a and b, each Li^+ eliminates two-thirds of the vacant sites in basic spinel cell, which causes the tetragonal distortion removal ($c/3a \rightarrow 1$) and the Li^+ incorporation process can be indicated in this way.

TABLE II Occupation of both cation and vacant sites in γ-and δ-spinel lattices as well as corresponding tetragonal distorsion of spinel cells. Compilation was performed using the Wilson [2] and Wilson and McConnell [12] data

Alumina compound	(c/a) or $(c/3a)$	Vacancies ordering	Octahedral (O) or tetrahedral (T) sites		
			Available	Occupied by Al	Vacant
γ-Al_2O_3	0.985	Tetrahhedral	16(O)	16(O)	–
			8(T)	16/3(T)	8/3(T)
γ-Al_2O_3	0.991	Random	16(O)	128/9(O)	16/9(O)
			8(T)	64/9(T)	8/9(T)
δ-Al_2O_3	0.981	Octahedral	16(O)	40/3(O)	8/3(O)
			8(T)	8(T)	–

γ(Li) phases can be characterized as the metastable intermediate spinel-like compounds in the δAl_2O_3–$LiAl_5O_8$ system where, as suggested from the IR spectroscopy measurements, the disordered octahedral cations distribution occurs. The basic spinel structure unit of γ(Li) can be assigned by the formula $Al_8[Al_{(40-x)/3}\square_{(8-2x)/3}Li_x]O_{32}$. The $\delta \rightarrow \gamma$(Li) transformation proceeds accordingly to scheme 2a by a simple ion exchange $Al^{3+} + 2\square = 3Li^+$ in the framework of the fcc sublattice O^{2-} which represent a favoured kinetic route. This renders the γ(Li) phase relatively stable, as the further transformation towards $LiAl_5O_8$ requires extensive cation sites rearrangement. That is why the $LiAl_5O_8$ formation stage has not been attained within the infiltration period and it seems much higher temperatures must be applied to accomplish the $\delta \rightarrow LiAl_5O_8$ transformation. As reported by Stork and Pott [18] on calcination of $Li_2CO_3/\gamma Al_2O_3$ catalyst (up to 1473 K), XRD lines due to $LiAl_5O_8$ did not appear below 1273 K, where $LiAl_5O_8$ is formed by interaction between intermediate Li_2O and γAl_2O_3 support, exhibiting in this way some similarity with our model conception.

A gradual disappearance of δAl_2O_3 superlattice, occurring to some degree already within an infiltration period, can be attributed to the beginning of γ(Li) $\rightarrow LiAl_5O_8$ transformation, which is fully

accomplished during the annealing period. By the annealing procedure, a thermodynamic equilibrium state is established with long-range 1:3 ordering in the occupancy of octahedral sites to form the ordered $LiAl_5O_8$ polymorphism, where each Li^+ ion is surrounded by six Al^{3+} ions as nearest-neighbour cations, whereas each Al^{2+} ion has, as its nearest-neighbour cations, four Al^{2+} and two Li^+ ions [19]. This ordering process is clearly manifested by comparison of IR spectra in Figs 4 and 5. Thermodynamical analysis performed using the JANAF tables [20], as well as data presented by Byker *et al.* [21] and Weirauch *et al.* [22] has shown that the following reactions can occur at 1000 K in the system under consideration

$$1/2Li_2O + 5/2Al_2O_3(\gamma) = LiAl_5O_8$$
$$\Delta G_{1000} = -101.9\,kJ\,mol^{-1} \quad (3)$$
$$1/2Li_2O + 1/2Al_2O_3(\gamma) = LiAlO_2$$
$$\Delta G_{1000} = -48.7\,kJ\,mol^{-1} \quad (4)$$
$$2/5Li_2O + 1/5LiAl_5O_8 = LiAlO_2$$
$$\Delta G_{1000} = -69.1\,kJ\,mol^{-1} \quad (5)$$

which suggests that $LiAl_5O_8$ and $LiAlO_2$ are stable phases at temperatures around 1000 K. As thermodynamic data for δAl_2O_3 are missing, the values for γAl_2O_3 were taken for calculations. In fact, in annealed SF, αAl_2O_3, $LiAl_5O_8$ and very probably also $LiAlO_2$ phases were identified depending on the lithium content. It can be assumed that during the annealing period, the incorporation of residual lithium from crystallite grain boundaries into spinel cells proceeded, so that in long-term infiltrated SF, $Li/Al \approx 0.25$–0.30 concentration ratio was detected, exceeding the stoichiometric value for $LiAl_5O_8$ compound. $LiAlO_2$ aluminate that was identified in parallel with $LiAl_5O_8$ spinel, could be formed by Reaction 5. On the other hand, both αAl_2O_3 and $LiAl_5O_8$ phases were identified after annealing in the short-term infiltrated SF with $Li/Al \approx 0.05$ concentration ratio, which suggests that Reaction 3 has preferentially proceeded.

Although a relatively large amount of magnesium was detected by the SIMS method in SF, the assumption concerning Mg^{2+} ions incorporation into γ(Li) cells during the infiltration process has not been confirmed experimentally. As stated by Kordes [23], in the spinel system $LiAl_5O_8$–$MgAl_2O_4$ an uninterrupted series of solid solutions exist with continuous cell parameters change. In annealed SF, the fcc $LiAl_5O_8$ spinel with cell parameter $a = 0.7905$ nm was detected, which exactly coincided with data reported for pure $LiAl_5O_8$ substance [11], i.e. even during the annealing procedure no significant incorporation of Mg^{2+} ions into spinel cells occurred. Moreover, the preliminary experiments by Auger electron spectroscopy performed by us on *in situ* fractured surfaces of SF occurring in Mg8Li matrix, have shown the tendency of magnesium to be accumulated on the alumina crystallite grain boundaries, which also suggests that magnesium did not tend to penetrate into the spinel lattice.

As seen, experimental results fit the starting model conception quite well. Nevertheless, at least two aspects of this conception should be corrected: (a) $LiAl_5O_8$ formation stage is not attained in SF within the infiltration period, and (b) the incorporation of magnesium into forming γ(Li) spinel seems to be unlikely.

5. Conclusions

The study of phase transformations taking place in SF during their infiltration with molten Mg8Li alloy performed by SIMS, XRD and IR spectroscopy methods leads to the following conclusions.

1. The SIMS measurements have shown that lithium penetrates very quickly into the entire SF volume, most likely by diffusion along δAl_2O_3 crystallite grain boundaries, attaining up to $Li/Al \approx 0.25$–0.30 concentration ratio.
2. Lithium is incorporated into the δAl_2O_3 lattice within the infiltration period, to form intermediate metastable spinel-like compounds, γ(Li), at which the basic spinel structure unit can be assigned by formula $Al_8\,[Al_{(40-x)/3}\square_{(8-2x)/3}Li_x]\,O_{32}$.
3. The thermodynamic equilibrium state is attained by further transformation $\gamma(Li) \rightarrow LiAl_5O_8$ during the long-term annealing process, when $LiAlO_2$ aluminate can also be formed in SF if the stoichiometric Li/Al ratio for $LiAl_5O_8$ substance is exceeded.
4. In parallel with lithium, magnesium also penetrates the SF interior, however, the Mg/Al concentration ratio in approximately one order magnitude lower than that of Li/Al. The incorporation of magnesium into γ(Li) or $LiAl_5O_8$ lattices has not been observed and it seems that magnesium is accumulated in oxidic form on the δAl_2O_3 crystallite grain boundaries.

Acknowledgements

This work was supported by the Grant Agency for Science of the Slovak Republic (Project 2/74/93). Dr J. Sturm is thanked for performing IR spectroscopy measurements at the IFW Dresden, and for stimulating discussion. For additional structure investigations of the materials under discussion, we thank our colleagues of the Department for X-Ray Structural Research, IFW Dresden.

References

1. T. W. CLYNE, M. G. BADER, G. R. CAPPLEMAN and P. A. HUBERT, *J. Mater. Sci.* **20** (1985) 85.
2. S. J. WILSON, *Proc. Brit. Ceram. Soc.* **28** (1979) 281.
3. B. C. LIPPENS and J. H. de BOER, *Acta Crystallogr.* **17** (1964) 1312.
4. J. F. MASON, C. M. WARWICK, P. J. SMITH, J. A. CHARLES and T. W. CLYNE. *J. Mater. Sci.* **24** (1989) 3934.
5. S. KŮDELA, V. GERGELY, A. SCHWEIGHOFER, S. BAUNACK, S. OSWALD and K. WETZIG, *ibid.*, **29** (1994) 5071.
6. G. R. CAPPLEMAN, J. F. WATTS and T. W. CLYNE, *ibid.* **20** (1985) 2159.

7. S. HAFNER and F. LAVES, *Z. Kristallogr.* **115** (1961) 321.
8. P. TARTE, *Spectrochim. Acta* **23A** (1967) 2127.
9. W. J. PRICE, in "Laboratory methods in infrared spectroscopy", edited by R. G. J. Miller and B. C. Stace (Heyden, London, 1972) p. 97.
10. P. TARTE, *Compt. Rend. Acad. Sci.* **254** (1962) 2008.
11. R. K. DATTA and R. ROY, *J. Am. Ceram. Soc.* **46** (1963) 388.
12. S. J. WILSON and J. D. C. McCONNELL, *J. Solid State Chem.* **34** (1980) 315.
13. H. REMY, "Handbook of Inorganic Chemistry-Part 1" (Akademische Verlagsgesellschaft Geest & Portig K. -G., Leipzig, 1961) in German.
14. R. M. LEVY and D. J. BAUER, *J. Catal.* **9** (1967) 76.
15. E. J. W. VERWEY and E. L. HEILMANN, *J. Chem. Phys.* **15** (1947) 174.
16. A. -M. LEJUS and R. COLLONGUES, *Compt. Rend. Acad. Sci.* **254** (1962) 2005.
17. X. YANG, A. C. PIERRE and D. R. LIHLMANN, *J. Non-Cryst. Solids* **100** (1988) 371.
18. W. H. J. STORK and G. T. POTT, *J. Phys. Chem.* **78** (1974) 2496.
19. G. T. POTT and B. D. McNICOL, *J. Solid State Chem.* **7** (1973) 132.
20. "JANAF Thermochemical Tables", 2nd Edn, US Department of Commerce NSRDS-NBS, **37** (1971).
21. H. J. BYKER, I. ELIEZER, N. ELIEZER and R. A. HOWALD, *J. Phys. Chem.* **83** (1979) 2349.
22. D. A. WEIRAUCH and G. E. GRADDY, *J. Am. Ceram. Soc.* **75** (1992) 1484.
23. E. KORDES, *Z. Kristallogr.* **91** (1935) 193.

Received 27 May 1994
and accepted 8 September 1995